Clinical Proteomics

RESEARCH

Open Access

Integrated proteomics and *N*-glycoproteomic characterization of glioblastoma multiform revealed *N*-glycosylation heterogeneities as well as alterations in sialyation and fucosylation

Mingjun Hu[1,2], Kaiyue Xu[3], Ge Yang[3], Bo Yan[3], Qianqian Yang[3], Liang Wang[4], Shisheng Sun[3*] and Huijuan Wang[3*]

Abstract

Background Glioblastoma multiforme (GBM) is the most common malignant primary brain tumor. Notwithstanding tremendous efforts having been put in multi-omics research to profile the dysregulated molecular mechanisms and cellular pathways, there is still a lack of understanding about the glycoproteomic of GBM. Glycosylation as one of the most important post-translational modifications is crucial in regulating cell proliferation and relevant oncogenic pathways.

Results In the study, we systematically profiled *N*-glycoproteomics of para-cancerous and cancerous tissues from GBM patients to reveal the site-specific *N*-glycosylation pattern defined by intact glycopeptides. We identified and quantified 1863 distinct intact glycopeptides (IGPs) with 161 *N*-linked glycan compositions and 326 glycosites. There were 396 IGPs from 43 glycoproteins differed between adjacent tissues and GBM. Then, proteomic and glycoproteomic data were combined, and the normalized glycosylation alteration was calculated to determine whether the difference was attributed to the global protein levels or glycosylation. The altered glycosylation triggered by site-specific *N*-glycans and glycoprotein abundance, as well as glycosite heterogeneity, were demonstrated. Ultimately, an examination of the overall glycosylation levels revealed a positive contribution of sialylated or/and fucosylated glycans.

Conclusions Overall, the dataset highlighted molecular complexity and distinct profiling at translational and post-translational levels, providing valuable information for novel therapeutic approaches and specific detection strategies.

Keywords Glioblastoma multiform, Proteomics, Intact glycopeptides, *N*-glycosylation heterogeneities, *N*-glycan

*Correspondence:
Shisheng Sun
suns@nwu.edu.cn
Huijuan Wang
whj@nwu.edu.cn
Full list of author information is available at the end of the article

Graphical Abstract

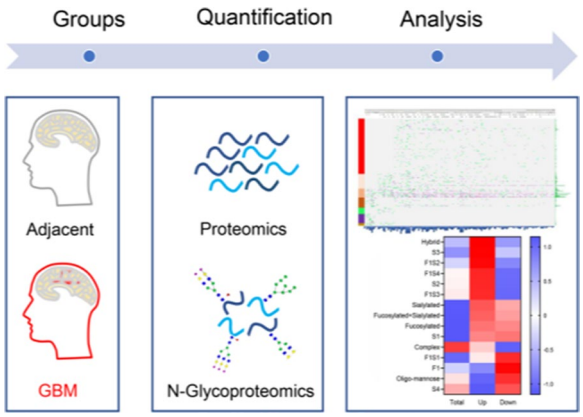

Background

Glioblastoma multiforme (GBM) is the most common and malignant form of primary brain tumors, characterized by rapid proliferation, diffuse infiltration and dismal prognosis [1, 2]. Despite the current standard treatment implicating surgical resection followed by radiotherapy with concomitant alkylating agent temozolomide (TMZ) chemotherapy established, progress in the treatment of GBM and long-term survival rates for patients remain dismal. The median progression-free survival for patients is 6.2 to 7.5 months, and the median overall survival from diagnosis is 14.6 to 16.7 months [3, 4]. As consequence, profiling the dysregulated molecular mechanism and cellular pathways to probe targets for novel therapies and ultimately improve the prognosis is extremely grim.

Notwithstanding tremendous efforts having been put in multi-omics research, it's still a relative lack of understanding about the glycoproteomic of GBM. Glycosylation, as one of the most important post-translational modifications (PTMs), plays an indispensable role in regulating cell proliferation and relevant oncogenic pathways, in concert with facilitating tumor-induced immunomodulation and eventual metastasis [5, 6]. Aberrant glycosylation because of alteration in some protein functions associated with abnormal glycosylation, including some glycosylation-related enzymes and glycosylated proteins, may be closely related to the relevant biological behaviors of glioma cells. Fabris et al. characterized the natural ganglioside mixture from GBM multiforme, corresponding peritumoral tissues and healthy human brain, founding ganglioside expression was significantly changed in GBM compared with healthy brain tissue [7]. Sethi et al. performed in-depth glycoproteomic analysis of the matrix and its components in control and GBM samples, including proteoglycans and glycosaminoglycans. The results uncovered that glycosylation was higher in GBM compared with control samples, coupled with glycosyltransferase and glycosidase expression levels upregulated [8]. Elevated in β1,6-*N*-acetylglucosaminyl transferase (GnT-V) and the resulting increase in β1,6-*N*-linked glycan branching lessened cell–cell and cell–matrix adhesion as well as enhanced migration and invasion [9, 10]. Additionally, high levels of cell-surface α−2,3-linked terminal sialic acids on glycoproteins in human gliomas affected tumor growth, escape from apoptosis, metastasis formation, and resistance to therapy [10, 11], while α−2,3-sialyltransferase inhibition caused an impairment of interactions with extracellular matrix (ECM) components and migratory capacity [12]. Moreover, the structural and functional changes of glycosylation-related enzymes or related proteins were working through cell–matrix or cell–cell interactions, and triggering downstream pathways [13]. A study constructed a functional glyco-model based nine glycosylation regulators screened from TCGA databases to predict glioblastoma outcomes and therapy responsiveness. The model indicated that patients from high-risk subgroups based on target glycosyltransferases are strongly related to an unfavorable immunosuppression and prognosis compared with the lower subgroup [14]. The researchers characterized the impact of aberrant glycosylation on cell biology in a broad panel of high- and low-grade glioma cell lines, suggesting that the four high-grade glioma cell lines (LN229, U87MG, U251 and U373) presented a similar profile with high abundance of sialylated N-glycans. Moreover, SLe^x as one of the members of the Lewis glycan family, was over-expressed in six high-grade glioma cell lines (A172, U118, U251, U373, T98G and LN229).

Downmodulation of *N*-glycosylation by treatment with *N*-glycosylation inhibitors in LN229 cell line decreased SLe^x expression, together with cell adhesion and migration [15]. A further investigation on integrated profiling of proteome and *N*-glycosylation, along with site-specific glycosylation changes has the potential for understanding the biological characteristics and developing therapeutic targets of GBM.

Herein, we performed integrated proteomic and *N*-glycoproteomic analyses of three non-paired GBM and adjacent tissue samples to investigate the different abundance in glycoprotein and site-specific *N*-glycosylation defined by intact glycopeptides pattern. At the outset, comprehensive profiling of site-specific *N*-glycosylation was delineated, followed by a deeper characterization of the discrepant analysis on the enriched function of differently expressed glycopeptides elucidated. Furthermore, altered glycosylation triggered by site-specific *N*-glycans and glycoprotein abundance, along with heterogeneity on glycosites of GBM were revealed by the integrated analyses. Mapping the altered glycosylation pattern among proteins in GBM and adjacent tissue to a certain extent sheds light on therapeutic targets and biomarkers, as well as a better understanding of disease pathogenesis.

Materials and methods

Protein extraction and tryptic digestion

Each three GBM and adjacent tissue samples used in the study were obtained from patients in the Tangdu Hospital of Air Force Medical University (China). The study was approved by the Ethics Committee of the Tangdu Hospital of the Air Force Medical University, and all patients have signed the informed consent. The clinical diagnostic results are shown in Supplementary Table 1 (Table S1).

The frozen brain tissues were denatured in homogenized separately in lysis buffer (8 M urea, 1.0 M NH_4HCO_3, pH 8.0) by sonication. Lysates were precleared by centrifugation, followed by protein concentrations determined by BCA assay. Proteins were reduced with 5 mM dithiothreitol for 1 h at 37 °C and subsequently alkylated with 15 mM iodoacetamide for 30 min at room temperature (RT) in the dark. Samples were digested with sequencing grade modified trypsin (Promega) at a 1:100 enzyme-to-substrate ratio for 2 h at 37 °C with shaking. Another aliquot of the same amount of trypsin was added to the samples and incubated at 37 °C overnight. The digested samples were then acidified with 1% trifluoroacetic acid (TFA) to pH < 2 and centrifuged. The supernatant was desalted on Oasis HLB columns (Waters) and eluted by 50% acetonitrile (ACN)/0.1% TFA solution. The peptide concentration was measured by BCA combined with the ultra-micro dual determination.

Enrichment of intact glycopeptides by mixed anion-exchange

The Mixed Anion-Exchange (MAX) columns (30 mg, Waters) were equilibrated successively with 100%ACN, 100 mM triethylammonium acetate, water, and 95% ACN/1% TFA, three times each. Then the intact glycopeptides enriched by MAX columns were adjusted to a solvent of 95%ACN/1%TFA. Peptides were loaded onto MAX columns and washed four times with 95% ACN/1% TFA. Bound enriched glycopeptides were eluted twice in 200 μL of 50% ACN/0.1% TFA, then dried by vacuum and resuspended in 0.1% TFA solution for liquid chromatography-tandem MS (LC–MS/MS) analysis.

LC–MS/MS analysis

The peptide and intact glycopeptide samples were separated on an Easy- nLC™ 1200 system (Thermo Fisher Scientific) with a 75 μm × 50 cm Acclaim PepMap100 C18 column protected by a 75 μm × 2 cm guard column. The mobile phase flow rate was 300 nL/min and consisted of 0.1% formic acid (FA) in water (A) and 0.1% FA in 80% ACN (B). The gradient profile was set as follows: 3–7% B for 1 min, 7–35% B for 90 min, 35–68% B for 19 min, 68–100% B for 1 min and equilibrated in 100% B for 9 min. MS analysis was performed using an Orbitrap Fusion Lumos mass spectrometer (Thermo Fisher Scientific). The MS parameters were as followed: spray voltage was 2.4 kV; Orbitrap MS1 spectra (AGC 4×10^5) were collected from 350 to 2000 m/z at a resolution of 60 K coupled with data-dependent higher-energy collision dissociation (HCD) MS/MS spectra at a resolution of 50 K; ions selected for MS/MS were separated at a width of 1.6 Da and fragmented using a collision energy of 35%. The fragments of peptides with charge states from 2 to 8 were screened. A dynamic exclusion time of 25 s was used to discriminate against previously analyzed ions.

Identification and quantification of global proteins

Data of global proteins were searched using SEQUEST in Proteome Discover 2.3 (Thermo Scientific) against the uniport human protein databases downloaded from http://www.uniprot.org in June 2019. Peptides were searched with up to two missed cleavages for trypsin digestion. The partially tryptic search used a 10 ppm precursor ion tolerance, 0.02 Da fragment ion tolerance. Static carbamidomethylation (C, + 57.0215 Da) on Cys residues, dynamic oxidation (+ 15.9949 Da) on Met residues, and *N*-terminal acetylation (+ 42.0106 Da) were set for searching the global proteome data. Peptide identification stringency was filtered with a 1% false discovery rate threshold (FDR) at the peptide-spectrum match (PSM) level. The relative protein

abundance was performed by label-free quantification (LFQ). Protein intensities were normalized to the peptide amount of the corresponding dataset to minimize possible variation between analyses [16].

Identification and quantification of intact glycopeptides

Before intact glycopeptide identification, Trans-Proteome pipline (TPP) was applied to convert the.RAW files to.mzML format, followed by searched using GPQuest 2.0 software. The MS/MS spectra containing at least two oxonium ions (m/z 204.0966) in the top 10 fragment ions were considered as the potential glycopeptide candidates. Mass tolerances of 10 and 20 ppm were allowed for precursors and fragmentation ions, respectively. The FDR of identified intact glycopeptides was estimated by the decoy peptide method, and 1% FDR was reserved as qualified identifications. The site-specific *N*-glycan structures on glycopeptides were further determined by glycopeptide analysis software StrucGP (https://github.com/Sun-GlycoLab/StrucGP), with the same searching parameters as that for proteomic data using the human UniProt database.

The quantification information of intact glycopeptides was extracted from MaxQuant results based on identified MS/MS scan numbers. The MS/MS spectra contain a maximum of two missed cleavage sites for trypsin digestion. The precursor mass tolerance was set as 5 ppm, and the fragment mass tolerance was 20 ppm. The rest parameters were the same as the global protein identified. Glycopeptides were quantified by LFQ. Intact glycopeptides intensities were normalized to the peptide amount of the corresponding dataset to minimize possible variation between analyses. The relative abundances of intact glycopeptides of samples were normalized to the median glycopeptides intensity in each corresponding sample. The identified intact glycopeptides with at least 5 PSMs were filtered and the medium ratio of each glycopeptide was used for its quantitation.

Lectin blot

Tissue samples were immersed in the RIPA buffer (HAT, China) in the presence of 1% PMSF and 1% inhibitor, and were lysed after ultrasonic decomposition on ice. The supernatant was collected after high-speed centrifugation. Equal amounts of total protein were separated on 10% SDS-PAGE gradient gels and transferred to PVDF membranes. Membranes were blocked with 1×Carbo-free blocking buffer (Vectorlabs, America) and then incubated with lectins at 4 ℃ overnight. Blots were washed and analyzed on Image System.

Bioinformatic analysis

The Gene Ontology (Go) and Kyoto Encyclopedia of Genes and Genomes (KEGG) enrichment analysis were displayed in Metascape (https://metascape.org/). The volcano plot and hierarchical clustering heatmap were constructed by Origin 2019.

Results

Quantitative analysis of intact glycopeptides between GBM and adjacent tissues

The integrated proteomic and glycoproteomic analyses of three non-paired GBM and adjacent tissue samples were presented to delineate the different glycosylation and altered glycosylation enzymes. The label-free quantification (LFQ) method was applied for the analysis of proteins and intact glycopeptides (IGPs). To eliminate variation caused by sample preparation, part of the trypsin-digested peptides was directly analyzed by mass spectrometry (MS) for global proteome analysis. The remanent peptides were used to enrich intact glycopeptides (IGPs) by mixed anion-exchange (MAX) cartridges, followed by identification of the glycans occupying those *N*-linked sites with GPQuest software (Fig. 1A).

A total of 1863 glycopeptides were identified in adjacent and GBM tissues samples. Among the 1863 *N*-linked IGPs, 1129 glycopeptides were both identified in the two groups (Table S2, Table S3). Compared to the adjacent group, 413 glycopeptides were only found in the GBM group. Similarly, 321 glycopeptides were unique in the adjacent group (Fig. 1B). The IGPs contain 161 *N*-linked glycan compositions modified at 326 unique glycosites from 82 glycoproteins, most of the glycosite-containing peptides (96%) including an *N*-X-S/T motif (X represents any amino acid apart from proline). Among the 161 *N*-glycan compositions, most (127, 78.9%) were complex glycans, hybrid (13, 8.1%), and oligo-mannose (11, 6.8%) glycans followed (Fig. 1C). The subtype of the other ten glycans was labeled as 'other' on account of the insufficient information.

Site-specific *N*-glycosylation profiling in GBM and adjacent tissues

To delineate the comprehensive profiling of site-specific *N*-glycosylation in GBM and adjacent tissues, IGPs corresponding to the specific glycosites and glycan composition, as well as the number of PSMs, were presented in Fig. 2A. Based on the peptide backbone of IGPs, almost half (151, 51.7%) of the glycosites were only occupied by complex glycans followed by a combination of complex and hybrid (40, 13.7%), and 24 glycosites (8.2%) were

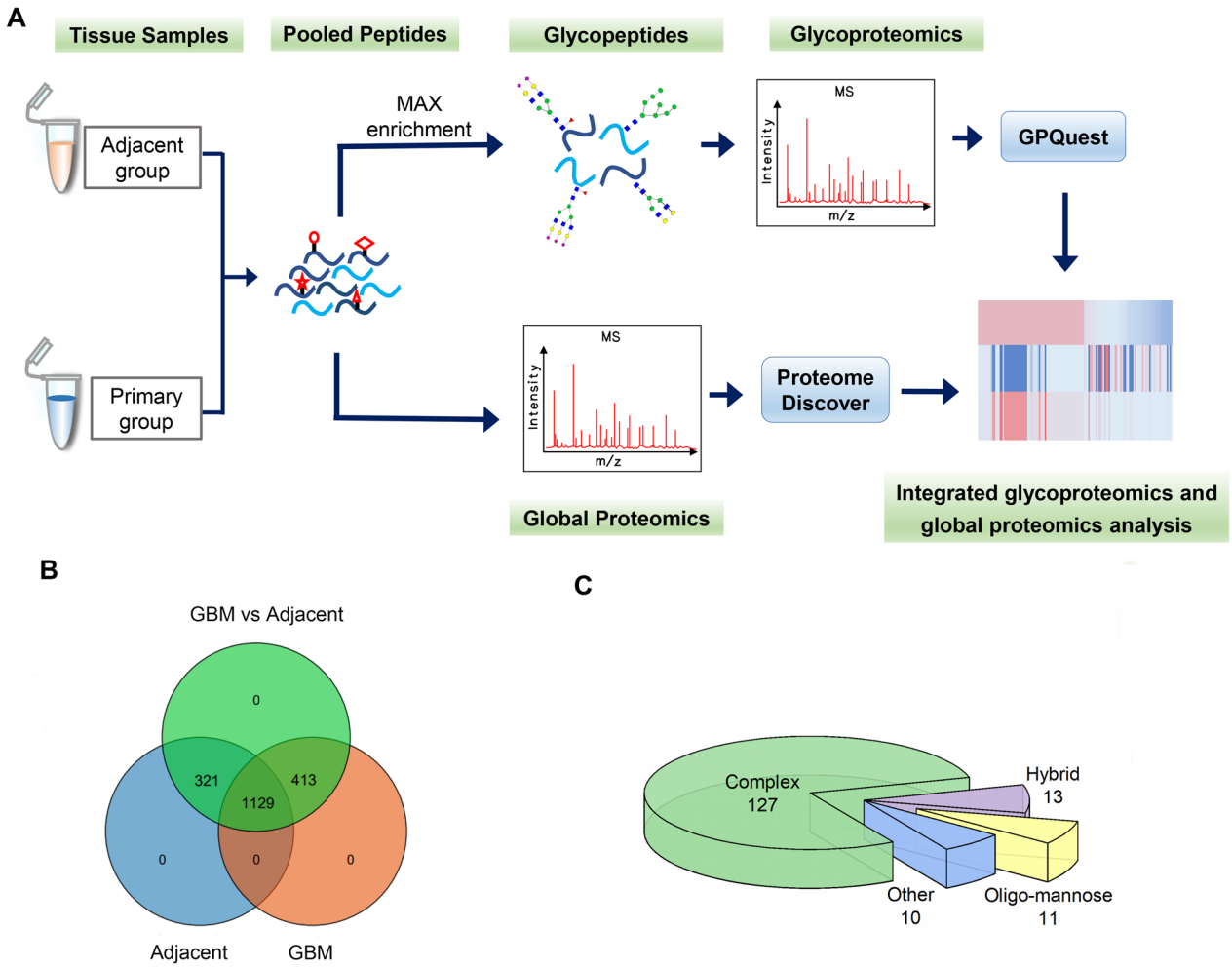

Fig. 1 Quantitative analysis of integrated intact glycoproteomic and proteomic strategy between GBM and adjacent tissues. **A** Schematic representation of the workflow for integrated proteome and glycoproteome. Proteins from 3 non-paired GBM tissues and non-tumor tissues were extracted and digested into peptides, which were analyzed by global proteomics. Intact glycopeptides (IGPs) were enriched by mixed anion-exchange (MAX) from the peptides and analyzed using LC–MS/MS, followed by identified and quantified using GPQuest for site-specific glycosylation. **B** Venn diagram of the identified IGPs in GBM and adjacent group. **C** Quantitative statistics of three glycan types attached to IGPs

modified by a combination of all three different types of glycan (Fig. 2A).

When taking into the counts of PSMs of each glycan type, we found that the vast majority of glycosites (5722, 88.3%) were modified by complex glycans, followed by hybrid (445, 6.9%) and oligo-mannose (311, 5.4%) glycans. Furthermore, 55.2, 65.9 and 40.4% of the glycosites were occupied by fucosylated glycans (Fuc), sialylated glycans (Sia) and both glycans, respectively (Fig. 2B). The number of glycosites modified by each glycan type was also gathered, and the results indicated that each glycan had at least one glycosite, some even up to 32. The types of glycans by which the number of glycosites in the top ten were occupied were listed (N4H5S2, N4H5F1S1, N4H5F1S2, N4H4F1S1, N4H5S1, N2H8, N6H3F1S1, N6H3F1S2, N6H4, N5H5F1S1) (Fig. 2C).

For the same protein, the specific glycosite is diverse probably given the difference in the structure of linked-glycans. The analysis of the glycan types at each glycosylation site elucidated that 5/8 of (182, 62.3%) glycosites were modified by at least two glycans, and 12 of them even contained more than 20 different glycan types (Fig. 2A). Moreover, the variety of glycan compositions that are bound to specific or different glycosites in the same protein, named site heterogeneity, was uncovered. In the case of the three glycosites from epidermal growth factor receptor (EGFR), one glycosites (Asn-109) was modified by three types of complex glycans; glycosites

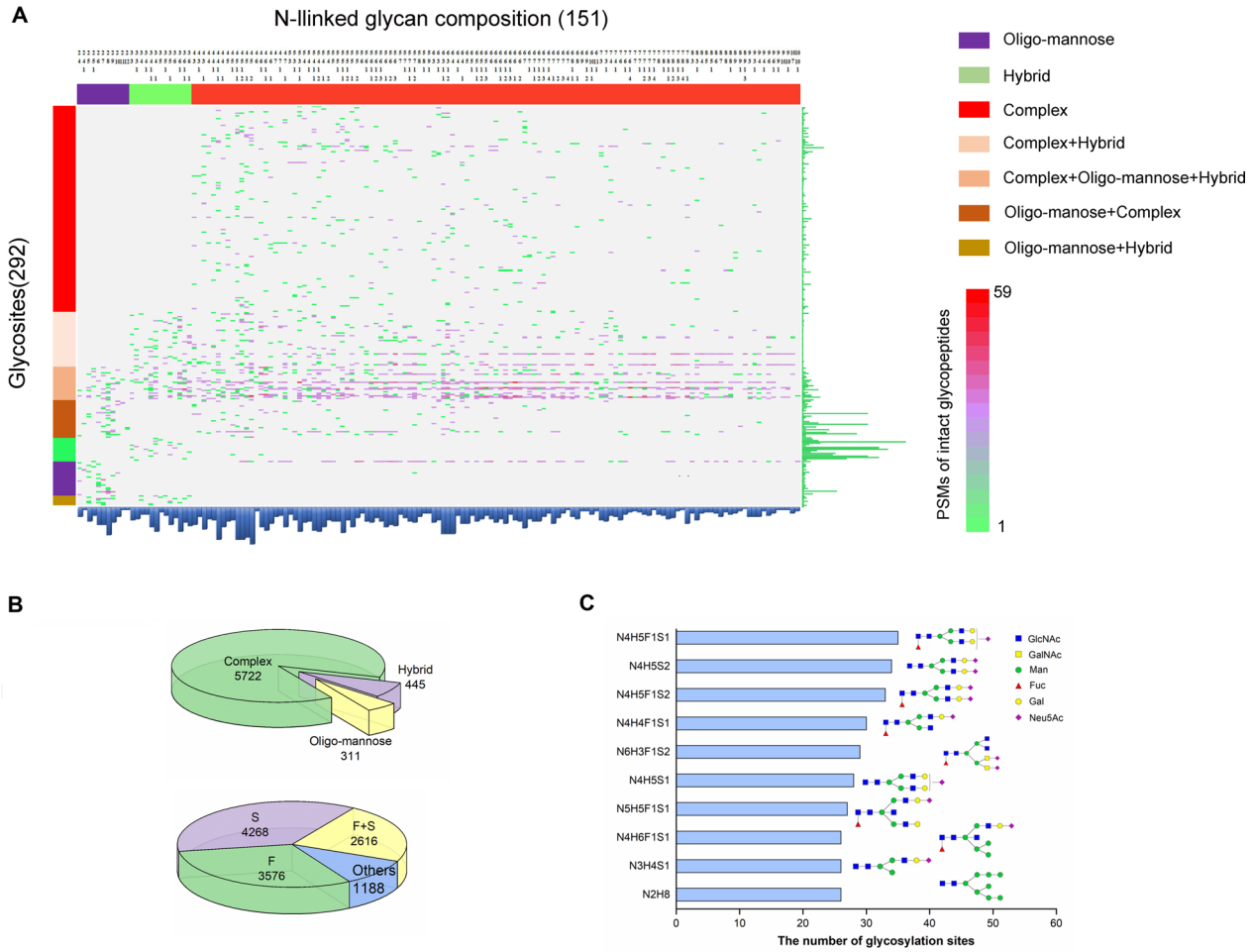

Fig. 2 Site-specific *N*-glycosylation profiling in GBM and adjacent tissues. **A** A comprehensive delineation of identified IGPs, glycan types, glycosylation site, and the number of PSMs. Each *N*-glycan composition (upper) and glycosite (left) included in IGPs were represented. The amount of glycosites corresponding to each *N*-glycan composition (below) and glycans attached to each glycosite (right) was also displayed. The number of PSMs was indicated in the middle of the heatmap. **B** PSMs of glycan types and sialic acid or fucose. **C** The top ten glycans with the highest number of glycosites

Asn-347 and Asn-594 were both occupied by two types of complex glycans.

A discrepant analysis on the enriched function of differently expressed glycopeptides in GBM

To improve quantitative accuracy determined by the LFQ method, the quantified IGPs were further filtered with the number of PSMs greater than or equal to 5, and unknown glycans due to the lack of mass spectra data were also excluded. Thus, 396 intact glycopeptides from 43 glycoproteins were identified in adjacent tissues and GBM. According to the cutoff of significant changes (fold change ≥ 2), the differentially expressed IGPs accounted for a substantial part with 73.5% (Fig. 3A). Among them, 153 IGPs were dramatically elevated in GBM compared with adjacent tissues, while 138 IGPs were significantly restrained (Fig. 3B). The up-regulated or down-regulated glycopeptides were clustered into two parts, contained only in the GBM group and embraced in both (Fig. 3C).

In addition, the KEGG pathway and GO analysis were applied on the significant IGPs in GBM based on their corresponding proteins. As shown in Fig. 3D, 13 overlapped proteins were observed between the 24 proteins from upregulated IGPs and 28 proteins from downregulated IGPs, along with the different proteins falling into the same ontology term. The KEGG enrichment analysis on differentially expressed IGPs indicated that ECM-receptor interaction, ECM proteoglycans, extracellular matrix organization and integrin cell surface interactions were the overrepresented pathway in both up- and down-regulated IGPs. However, the PI3K-Akt signaling pathway was the significantly overrepresented pathway for the upregulated IGPs, while heterotypic cell–cell adhesion was the top overrepresented pathway among the

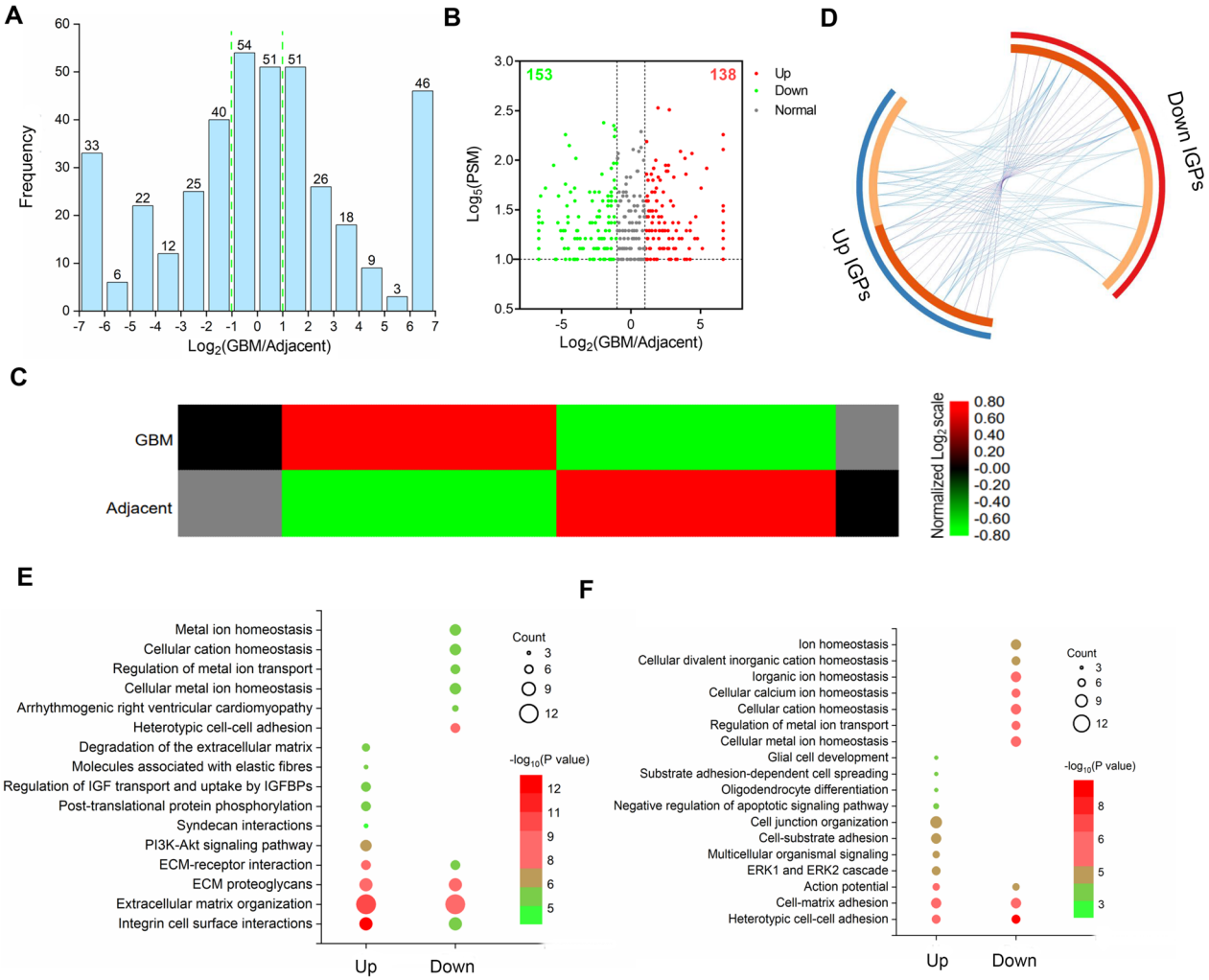

Fig. 3 A discrepant analysis on the enriched function of differently expressed glycopeptides in GBM. **A** Frequency distribution histogram of fold change between GBM and adjacent tissues. **B** The volcano map of differently expressed glycopeptides. Red and green dots represented upregulated and down-regulated glycopeptides based on the value of log2(GBM/Adjacent), respectively. **C** Heatmap of the differently expressed glycopeptides. Blank indicated the glycopeptides were solely identified in one group, and gray represented a blank value. **D** Circos map of overlapped proteins observed from upregulated and downregulated IGPs. The blue and red outer arcs represented proteins that upregulated and downregulated IGPs corresponded to, respectively. The light orange inner circle indicated that proteins were unique to this list, and the dark orange indicated the overlapped protein between the lists. The purple line showed the overlapped proteins, and the blue line showed the functional correlation between the proteins. **E** KEGG pathway and **F** molecular function analysis of 396 IGPs from 43 glycoproteins

downregulated IGPs (Fig. 3E). GO analysis indicated that those IGPs were primarily implicated in heterotypic cell–cell adhesion, cell–matrix adhesion and action potential. The top molecular function, ERK1 and ERK2 cascade uniquely enriched in up-regulated glycoproteins was observed, and cellular metal ion homeostasis was notably enriched in downregulated IGPs (Fig. 3F).

Integrated glycoproteomic analysis revealed alterations in glycosylation sites and site-specific glycans of GBM

To further determine whether the difference was attributed to the global protein levels or glycosylation of the glycosylation site and glycan types, the alteration in the levels of IGPs and corresponding proteins was contrasted. The normalized glycosylation alteration was calculated by dividing glycopeptides ratios by corresponding proteins ratios (Table S3). A large number of glycopeptides (174, 43.9%) were outside of the 0.5 and 2 intervals in GBM. Among the 174 *N*-glycopeptides, 34 glycopeptides only altered at protein levels with the fold change of protein more than 2 and glycopeptides less than 2. Likewise, 45 glycopeptides solely changed at glycosylation level, combined with 127 glycopeptides altered at both levels (Fig. 4A). The data indicated that glycosylation

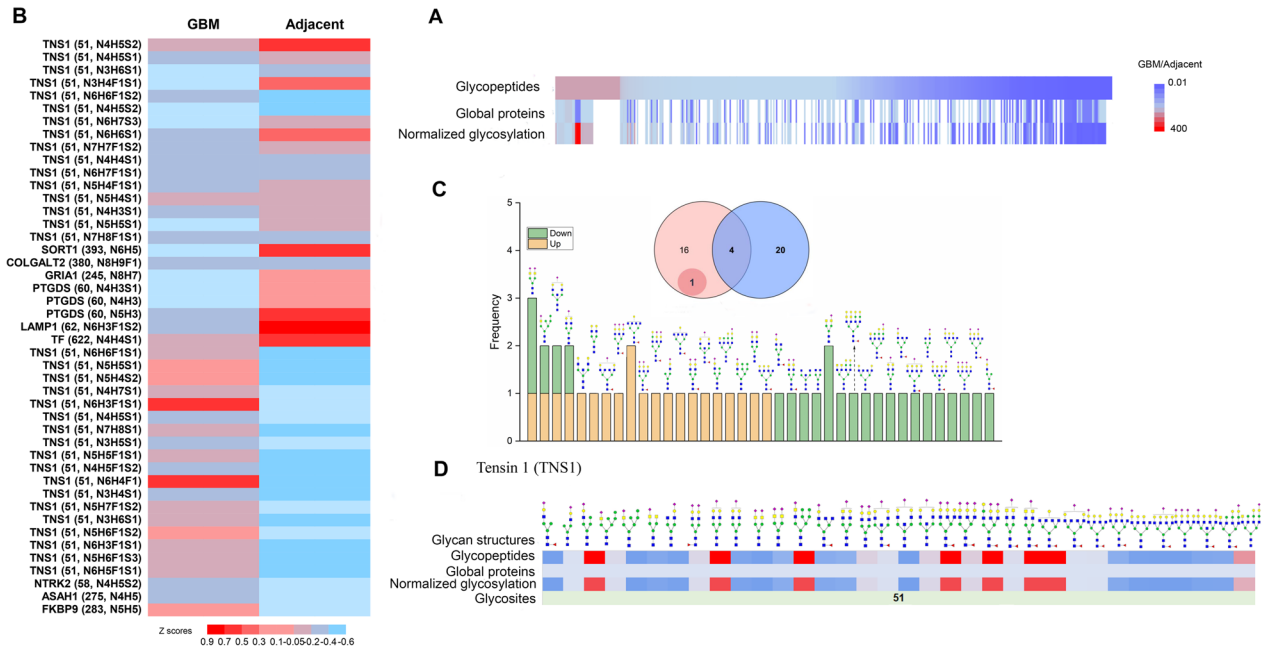

Fig. 4 Integrated proteomic and glycoproteomic analysis of altered IGPs and corresponding proteins in GBM. **A** Heatmap of the altered fold change of glycopeptides and corresponding proteins, as well as the normalized glycosylation alteration calculated by dividing glycopeptides ratios by corresponding proteins ratios. **B** Heat map of glycopeptides solely changed at glycosylation level with a *z*-scored abundance. **C** Frequency of site-specific glycans in altered glycopeptides between GBM and adjacent tissues. **D** The site-specific *N*-glycan of glycosites from glycoprotein with no significant change in the protein level, Neurotrophic receptor tyrosine kinase 2 (NTRK2) and Tensin 1 (TNS1)

occupancy, as well as protein abundance level, should make explanation conjointly for the significant changes of glycoproteins.

The 45 glycopeptides solely changed at glycosylation level including 21 increased and 24 decreased glycopeptides, which consisted of 38 glycans and 10 glycosites (Fig. 4B). Among the 38 glycans, 4 glycans were included in both up-and down-regulated glycopeptides, 20 and 22 glycans in up-and down-regulated glycopeptides respectively. The glycans with sialic acid (N4H5S2, N3H6S1, N5H5S1 and N4H5S1) were found in both up- and down-regulated glycopeptides. Furthermore, the hybrid glycans (N3H4S1 and N3H5S1) with sialic acid were occurred in the upregulated glycopeptides, while hybrid glycan (N3H4F1S1) in the downregulated glycopeptides was both sialylated and core-fucosylated. Additionally, glycopeptides modified by tri-antennary glycan were primarily elevated, together with tri-antennary glycan containing core fucose presented uniquely. Glycopeptides modified by tetra-antennary glycan comprising both sialic acid and fucose were only focused on the upregulated (Fig. 4C).

Notably, although parts of differential abundance alteration of glycosite-containing peptides had a positive relationship with the corresponding global protein expression, the abundance changes of glycosites of certain glycoproteins could display diacritical expression patterns from their global levels. Neurotrophic receptor tyrosine kinase 2 (NTRK2), for example, showed a protein abundance of 1.38, indicating no significant change in the protein level. Nevertheless, the observed glycosite of NTRK_Asn-58, solely identified in GBM contrasted to adjacent tissues, was determined to present extremely differential levels. The results uncovered that the abundance changes of glycoproteins were regulated by the glycosylation site occupancy level. Additionally, Tensin 1 (TNS1) also embraced a subset of complex and hybrid glycans that displayed significant variation in GBM except for significant discrepancy in the glycosite Asn-51, which revealed the influence of glycans types at the glycosite on abundance alteration of glycoproteins (Fig. 4D). Conclusively, the protein levels might be insufficient to explore the biomarkers and illuminate the potential mechanism of tumorigenesis, while the altered glycosylation levels on account of the extent of glycosylation or glycans types at the glycosite could be superior to protein abundance in diagnosis and surveillance of GBM.

Altered sialylation and core fucosylation in GBM

To figure out the discrepant profile of overall glycosylation levels, the number of glycopeptides modified by three glycan types was tallied, followed by the proportion of each glycan subtype that accounted for

calculated in quantified glycopeptides and differentially expressed glycopeptides. In the 396 quantified IGPs, the complex glycans were responsible for 87.6% with the highest proportion, the hybrid glycans immediately followed (7.7%) and then oligo-mannose glycans (4.7%). Against such a backdrop, the fucosylated or/and sialylated glycans were further analyzed, and the data elucidated it was in both upregulated and downregulated glycopeptides that the proportion of sialylated glycans, core-fucosylated glycans and both glycan all had a striking increase (Fig. 5A).

In an attempt to shed some light on the cause of altered glycans with sialic acid and/or fucose, the number of glycans consisting of varying amounts of sialic acid or/and core fucose was counted, as well as the corresponding percentage calculated. As shown in Fig. 5B, a higher proportion of fucosylated glycans without sialic acid (F1) was displayed in downregulated glycopeptides. The increase in proportion of glycans with one fucose and one sialic acid (F1S1) was observed in both up- and downregulated glycans. The percentage of other glycans containing fucose and sialic acids (F1S2 and F1S3) were elevated apparently in upregulated glycopeptides. Besides, the increased proportion of only sialylated glycans (S2) was observed in upregulated glycopeptides.

A comprehensive description of aberrant glycosylation was exhibited after the above results were integrated (Fig. 5C). The heatmap represented that the ratio of fucosylated and/or sialylated glycans were increased in up- and downregulated glycopeptides contrasted to quantified glycopeptides, suggesting an overall increase of fucosylation and sialylation in GBM. The LTL as one of lectins recognizing fucose was used, and the data indicated an up-regulation of fucose levels in small molecular weight proteins in GBM. The lectins (MAL-II and SNA) binding specifically to sialic acids were used, and the results of lectin blot suggested that the structure of Siaα2-3Galβ1-4Glc (NAc) recognized by MAL-II was slightly downregulated in GBM. However, the structure of Siaα2-6Galβ1-4GlcNAc recognized by SNA was elevated in GBM, which might account for the increased levels of sialic acids (Fig. 5D). Together, the decreased proportion of complex glycans in up- and downregulated glycopeptides contrasted to quantified glycopeptides indicated a whole reduction in GBM. The lectin (PHA-E + L) recognizing complex glycans was applied in lectin blot, and the result demonstrated its downregulation in GBM (Fig. 5D).

Additionally, a proportional growth of sialylated glycans (S3 and S2), and with both sialic and core fucose

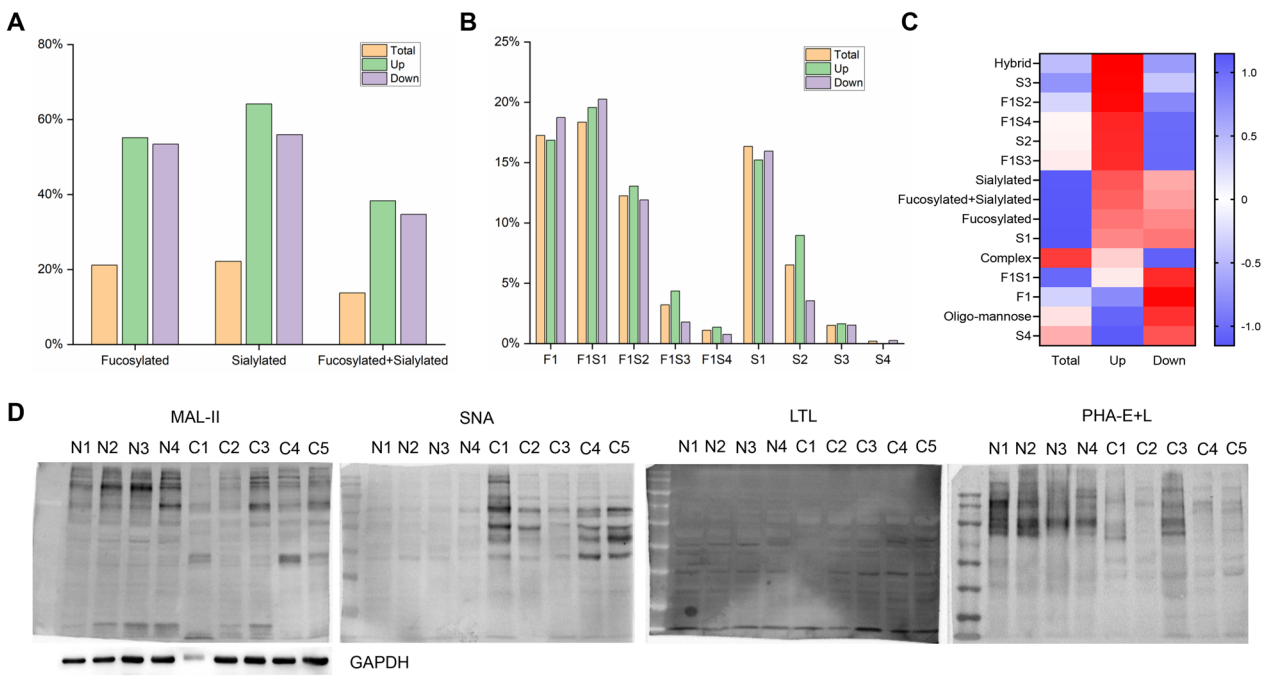

Fig. 5 The discrepant profile of overall glycosylation alteration. **A** The percentage of glycans including fucose and /or sialic acid, and corresponding amount (**B**). **C** Heatmap of all glycan types. Each row represented a glycan type, and the columns represented all qualified glycopeptides, upregulated and downregulated glycopeptides from left to right, respectively. **D** The results of lectin blot. The lectins (MAL-II and SNA) bind specifically to sialic acids, and the structure of Siaα2-3Galβ1-4Glc (NAc) and Siaα2-6Galβ1-4GlcNAc are recognized by MAL-II and SNA, respectively. The LTL as one of lectins recognizes core fucose. The lectin (PHA-E + L) recognizes complex glycans. N: adjacent tissues; C: GBM

(F1S2, F1S4 and F1S3) among upregulated glycans in GBM were illustrated from the whole increased ratio of fucosylated and/or sialylated glycans (Fig. 5C). The percentage increase in sialylated glycans (S4), together with fucosylated glycans (F1) and fucosylated & sialylated glycans (F1S1) among downregulated glycans in GBM, were also demonstrated the results mentioned above (Fig. 5C). Consequently, the elevated fucosylation and sialylation pinpointed in the integrated analysis of glycosylation changes were conspicuously contingent on multiple factors. Apart from the glycans including only fucose or sialic acids, glycans with both fucose and different amounts of sialic acids might account for the enhanced fucosylation and sialylation.

Discussion

Since nearly half of proteins are glycosylated in mammals, researches conducted on proteomics that aimed to delineate protein expression and the protein–protein network has certain limitations. Glycosylation, the most structurally diverse and complex post-translational modification, exerts a crucial biology role in cancer progression, including tumor invasion, cell infiltration and cell migration [6, 17, 18]. Several lines of evidence imply that the suitability of aberrant glycoproteins and glycans as attractive biomarkers and potential therapeutic targets of cancer progression continues to be delineated [19–21]. Consequently, we have contoured the comprehensive landscape of glycoproteomic profiling between GBM and adjacent tissues, revealing the site-specific *N*-glycosylation defined by intact glycopeptides pattern. Furthermore, a deeper characterization of the discrepant analysis on the enriched function of differently expressed glycopeptides in GBM was delineated. Ultimately, the contribution of sialylated or/and fucosylated glycans were analyzed. Overall, the dataset highlights the molecular complexity and distinct profiling at translational and post-translational levels.

In the study, a total of 1863 IGPs including 161 *N*-linked glycan compositions modified at 326 unique glycosites from 82 glycoproteins was identified and quantified from GBM and adjacent tissues samples. The microheterogeneity that multiple glycosites exist on specific glycoprotein, and a plethora of discrepant glycans modified at each glycosites [22, 23], potentiating the complexity of glycosylation, was uncovered. For instance, as the primary genetic markers for gliomas, genetic alterations in epidermal growth factor receptor (EGFR) are the dominant receptor tyrosine kinase lesions in GBM [24, 25]. The frequent EGFR vIII mutation might drive the aggressive nature of GBM by promoting invasion and angiogenesis [26]. Although protein expression of EGFR had no statistical difference in GBM compared with the adjacent group, the IGPs differed depending on the three glycosites modified by six different glycans. The uniquely identified glycan N5H5F1S1 and N6H7 in GBM might provide additional information for its causal role apart from genetic alterations.

Taking accuracy of determination by the LFQ method into consideration, significant IGPs with PSMs greater than 4 were selected to further study. To interrogate the discordantly functional relationship, the KEGG and GO analysis of IGPs based on corresponding genes revealed that differently expressed IGPs associated with cell–cell adhesion and cell–matrix adhesion, involved in ECM–receptor interaction, ECM proteoglycans and extracellular matrix organization pathways. A thick extracellular matrix (ECM) occupies the space between neurons and glial cells and comprises, facilitating GBM invasion by regulating the activity of proteolytic enzymes and epithelial-mesenchymal transition (EMT) [27, 28]. That is, the altered IGPs induced by site-specific glycans or glycosylation sites might be another fundamentally stimulated factor in GBM progression. Moreover, ERK1 and ERK2 cascade that participated in the Ras-Raf-MEK-ERK signal transduction, as well as significantly enriched PI3K-Akt signaling pathway among upregulated IGPs, both implicated in gliomagenesis and progression [29, 30]. Inversely, cellular metal ion homeostasis, such as Ca^{2+} signaling linked to metastasis and treatment outcomes in gliomas, was notably annotated among downregulated IGPs [31]. Interestingly, molecular function and enriched pathways of IGPs nearly all were contextualized to receptor tyrosine kinases (RTKs) signaling frequently altered in GBM, which energized investigations into the linkage of glycosylation with RTKs signaling in malignant GBM.

The integrated glycoproteomic analysis of global protein and glycosite-containing peptides illustrated that most of the changes in glycoproteins observed at protein expression were accompanied by altered glycosylation. Nevertheless, the abundance changes of glycosites from certain glycoproteins displayed diacritical expression patterns from their global protein levels, appearing to be caused by a change in the glycosylation site occupancy or glycans types at certain glycosite. Neurotrophic receptor tyrosine kinase 2 (NTRK2) without change in the protein level, its glycosite of NTRK_Asn-58 was solely identified in GBM. Quantification of certain protein glycosite specific to GBM could be helpful in diagnosis and surveillance.

In an attempt to explore the reasons leading to altered glycosylation levels, the analysis of enhanced sialylation and fucosylation was obtained. Hypersialylation promotes tumor cell invasion phenotype and tumor immune evasion, correlated with poor prognosis [32, 33]. Increased sialylation was confirmed in individuals with

cervical cancer cells [34]. Similarly, the *N*-glycan core fucosylation of EGFR regulated the EGFR-mediated signaling pathway, including cellular growth, and its interaction with EGF [35, 36]. Core fucosylation of integrin regulated its activity and mediated signal transduction related to cell migration and invasion [37, 38]. Here, we found the increased proportion of sialylation and fucosylation resulted from glycans including only fucose or sialic acids, together with glycans with both fucose and different amounts of sialic acids. Although four glycoproteins (FGB, COL6A3, BGN and FBN1) enriched in the ECM organization pathway both changed at proteins levels and glycosylation, the only identified fucosylated and sialylated glycans (N5H5F1S1, N6H3F1S1, N4H6F1S1, N6H3F1S2, N3H6S1, N3H6F1 and N6H4F1) and corresponding glycosites might mirror the combined effect of glycans on ECM and GBM development from another perspective. Integrins and growth factor receptors are both involved in ECM-cell interactions, and altered glycans and glycosites of ITGAV (N6H4 and N6H3) and EGFR (N5H5F1S1 and N6H7) in GBM further verified the above contents.

Conclusions

In conclusion, the integrated proteome and glycoproteomes analysis of GBM demonstrated the relationship between site-specific glycosylation and GBM, as well as revealed the insight gained by delineating prominent post-translational modification. We identified a combination of glycosylation sites and site-specific glycosylation from intact glycopeptides. Furthermore, an investigation of glycosylation showed that the differential glycoprotein expression arose from the differential extent of glycosylation and glycan types at glycosites. Ultimately, the increased sialylation and fucosylation glycans were a result of multiple factors, including glycans with only fucose or sialic acids and both fucose and different amounts of sialic acids. Overall, a comprehensive characterization of altering glycosylation in GBM has the potential for understanding the biological characterization and elucidating the pathogenesis, which provides scientific guidance for developing diagnostic and therapeutic targets of GBM. Whereas a small number of samples increases tumor heterogeneity to a certain degree, the results are insufficient to be convinced. As a result, we would collect additional samples to conduct additional research. Meanwhile, the study will be launched at the cellular level to further trace the cause of altered glycosylation, which will then be verified.

Abbreviations

GBM	Glioblastoma multiforme
IGPs	Intact glycopeptides
RT	Room temperature
MAX	Mixed Anion-Exchange
LC–MS/MS	Liquid chromatography-tandem MS
FA	Formic acid
HCD	Higher-energy collision dissociation
PSM	Peptide-spectrum match
LFQ	Label-free quantification
TPP	Trans-Proteome Pipline
KEGG	Kyoto Encyclopedia of Genes and Genomes
Fuc	Fucosylated glycans
Sia	Sialylated glycans
EGFR	Epidermal growth factor receptor
NTRK2	Neurotrophic receptor tyrosine kinase 2
TNS1	Tensin 1
ECM	Extracellular matrix
EMT	Epithelial-mesenchymal transition
RTKs	Receptor tyrosine kinases

Supplementary Information

The online version contains supplementary material available at https://doi.org/10.1186/s12014-025-09525-9.

Additional file 1.

Additional file 2.

Acknowledgements

We would like to thank everyone who contributed towards the article.

Author contributions

MH: conceptualization, methodology, investigation, data curation, writing, original draft preparation, funding acquisition; KX: conceptualization, formal analysis, investigation, writing, original draft preparation; GY: software and data curation; BY: software and data curation; QY: software and data curation; LW: formal analysis; SS: writing, review and editing, validation; HW: writing, review and editing, validation, funding acquisition. All authors read and approved the final manuscript.

Funding

This work was supported by the Natural Science Basic Research Program of Shaanxi (Program No. 2023-JC-YB-712), Xi'an Talent Program (XAYC210032) and Xi'an Science and Technology plan project (2024JH-YLYB-0451).

Availability of data and materials

The mass spectrometry proteomics data have been deposited to the ProteomeXchange Consortium (http://proteomecentral.proteomexchange.org) via the iProx partner repository [39] with the dataset identifier PXD029920.

Declarations

Ethics approval and consent to participate

The study was approved by the Ethics Committee of the Second Affiliated Hospital of the Air force Medical University (China), and all patients have signed the informed consent.

Consent for publication

Not applicable.

Competing interests

The authors declare no competing interests.

Author details

[1]Faculty of Life Sciences and Medicine, Northwest University Chang An Hospital, Northwest University, Xi'an 710069, Shaanxi, China. [2]Department of Neurosurgery, Chang An District Hospital, Xi'an 710118, Shaanxi, China. [3]National Engineering Research Center for Miniaturized Detection Systems, College of Life Sciences, Northwest University, Xi'an, Shaanxi, China. [4]Department of Neurosurgery, Tangdu Hospital of Air Force Medical University, Xi'an, Shaanxi, China.

Received: 2 August 2024 Accepted: 8 January 2025
Published online: 08 February 2025

References

1. Rousseau A, Mokhtari K, Duyckaerts C. The 2007 WHO classification of tumors of the central nervous system - what has changed? Curr Opin Neurol. 2008;21(6):720–7.
2. Poon CC, Sarkar S, Yong VW, Kelly JJP. Glioblastoma-associated microglia and macrophages: targets for therapies to improve prognosis. Brain. 2017;140(6):1548–60.
3. Stupp R, Hegi ME, Mason WP, van den Bent MJ, Taphoorn MJ, Janzer RC, Ludwin SK, Allgeier A, Fisher B, Belanger K, Hau P, Brandes AA, Gijtenbeek J, Marosi C, Vecht CJ, Mokhtari K, Wesseling P, Villa S, Eisenhauer E, Gorlia T, Weller M, Lacombe D, Cairncross JG, Mirimanoff RO, European Organisation for R, Treatment of Cancer Brain T, Radiation Oncology G, National Cancer Institute of Canada Clinical Trials G. Effects of radiotherapy with concomitant and adjuvant temozolomide versus radiotherapy alone on survival in glioblastoma in a randomised phase III study: 5-year analysis of the EORTC-NCIC trial. Lancet Oncol. 2009;10(5):459–66.
4. Stupp R, Taillibert S, Kanner A, Read W, Steinberg D, Lhermitte B, Toms S, Idbaih A, Ahluwalia MS, Fink K, Di Meco F, Lieberman F, Zhu J-J, Stragliotto G, Tran D, Brem S, Hottinger A, Kirson ED, Lavy-Shahaf G, Weinberg U, Kim C-Y, Paek S-H, Nicholas G, Bruna J, Hirte H, Weller M, Palti Y, Hegi ME, Ram Z. Effect of tumor-treating fields plus maintenance temozolomide vs maintenance temozolomide alone on survival in patients with glioblastoma: a randomized clinical trial. JAMA. 2017;318(23):2306–16.
5. Stowell SR, Ju T, Cummings RD. Protein glycosylation in cancer. Annu Rev Pathol. 2015;10:473–510.
6. Peixoto A, Relvas-Santos M, Azevedo R, Santos LL, Ferreira JA. Protein glycosylation and tumor microenvironment alterations driving cancer hallmarks. Front Oncol. 2019;9:380.
7. Fabris D, Rožman M, Sajko T, Vukelić Ž. Aberrant ganglioside composition in glioblastoma multiforme and peritumoral tissue: A mass spectrometry characterization. Biochimie. 2017;137:56–68.
8. Sethi MK, Downs M, Shao C, Hackett WE, Phillips JJ, Zaia J. In-depth matrisome and glycoproteomic analysis of human brain glioblastoma versus control tissue. Mol Cell Proteomics. 2022;21(4): 100216.
9. Yamamoto H, Swoger J, Greene S, Saito T, Hurh J, Sweeley C, Leestma J, Mkrdichian E, Cerullo L, Nishikawa A, Ihara Y, Taniguchi N, Moskal JR. Beta 1,6-N-acetylglucosamine-bearing N-glycans in human gliomas: implications for a role in regulating invasivity. Cancer Res. 2000;60(1):134–42.
10. Yamamoto H, Oviedo A, Sweeley C, Saito T, Moskal JR. Alpha 2,6-sialylation of cell-surface N-glycans inhibits glioma formation in vivo. Can Res. 2001;61(18):6822–9.
11. Büll C, Stoel MA, den Brok MH, Adema GJ. Sialic acids sweeten a tumor's life. Can Res. 2014;74(12):3199–204.
12. Büll C, Boltje TJ, Balneger N, Weischer SM, Wassink M, van Gemst JJ, Bloemendal VR, Boon L, van der Vlag J, Heise T, den Brok MH, Adema GJ. Sialic acid blockade suppresses tumor growth by enhancing T-cell-mediated tumor immunity. Can Res. 2018;78(13):3574–88.
13. Yue J, Huang R, Lan Z, Xiao B, Luo Z. Abnormal glycosylation in glioma: related changes in biology, biomarkers and targeted therapy. Biomarker Res. 2023;11(1):54.
14. Jin X, Chen Z, Zhao H. Deciphering glycosylation-driven prognostic insights and therapeutic prospects in glioblastoma through a comprehensive regulatory model. Front Oncol. 2014;14: 1288820.
15. Cuello HA, Ferreira GM, Gulino CA, Toledo AG, Segatori VI, Gabri MR. Terminally sialylated and fucosylated complex N-glycans are involved in the malignant behavior of high-grade glioma. Oncotarget. 2020;11:4822.
16. Kaiyue X, Kaiqian Z, Jiying M, Qianqian Y, Ge Y, Tingting Z, Guowei W, Bo Y, Jule S, Chao C, Liang W, Huijuan W. CKAP4-mediated activation of FOXM1 via phosphorylation pathways regulates malignant behavior of glioblastoma cells. Transl Oncol. 2023;29: 101628.
17. Reis CA, Osorio H, Silva L, Gomes C, David L. Alterations in glycosylation as biomarkers for cancer detection. J Clin Pathol. 2010;63(4):322–9.
18. Veillon L, Fakih C, Abou-El-Hassan H, Kobeissy F, Mechref Y. Glycosylation changes in brain cancer. ACS Chem Neurosci. 2018;9(1):51–72.
19. Munkley J, Vodak D, Livermore KE, James K, Wilson BT, Knight B, McCullagh P, McGrath J, Crundwell M, Harries LW, Leung HY, Robson CN, Mills IG, Rajan P, Elliott DJ. Glycosylation is an androgen-regulated process essential for prostate cancer cell viability. EBioMedicine. 2016;8:103–16.
20. Dimitroff CJ. I-branched carbohydrates as emerging effectors of malignant progression. Proc Natl Acad Sci USA. 2019;116(28):13729–37.
21. Munkley J. Glycosylation is a global target for androgen control in prostate cancer cells. Endocr Relat Cancer. 2017;24(3):R49–64.
22. Shah P, Wang X, Yang W, Toghi Eshghi S, Sun S, Hoti N, Chen L, Yang S, Pasay J, Rubin A, Zhang H. Integrated proteomic and glycoproteomic analyses of prostate cancer cells reveal glycoprotein alteration in protein abundance and glycosylation. Mol Cell Proteomics. 2015;14(10):2753–63.
23. Kolarich D, Jensen PH, Altmann F, Packer NH. Determination of site-specific glycan heterogeneity on glycoproteins. Nat Protoc. 2012;7(7):1285–98.
24. Brennan CW, Verhaak RGW, McKenna A, Campos B, Noushmehr H, Salama SR, Zheng S, Chakravarty D, Sanborn JZ, Berman SH, Beroukhim R, Bernard B, Wu C-J, Genovese G, Shmulevich I, Barnholtz-Sloan J, Zou L, Vegesna R, Shukla SA, Ciriello G, Yung WK, Zhang W, Sougnez C, Mikkelsen T, Aldape K, Bigner DD, Van Meir EG, Prados M, Sloan A, Black KL, Eschbacher J, Finocchiaro G, Friedman W, Andrews DW, Guha A, Iacocca M, O'Neill BP, Foltz G, Myers J, Weisenberger DJ, Penny R, Kucherlapati R, Perou CM, Hayes DN, Gibbs R, Marra M, Mills GB, Lander E, Spellman P, Wilson R, Sander C, Weinstein J, Meyerson M, Gabriel S, Laird PW, Haussler D, Getz G, Chin L, Network TR. The somatic genomic landscape of glioblastoma. Cell. 2013;155(2):462–77.
25. Bruford EA, Braschi B, Denny P, Jones TEM, Seal RL, Tweedie S. Guidelines for human gene nomenclature. Nat Genet. 2020;52(8):754–8.
26. Eskilsson E, Rosland GV, Talasila KM, Knappskog S, Keunen O, Sottoriva A, Foerster S, Solecki G, Taxt T, Jirik R, Fritah S, Harter PN, Välk K, Al Hossain J, Joseph JV, Jahedi R, Saed HS, Piccirillo SG, Spiteri I, Leiss L, Euskirchen P, Graziani G, Daubon T, Lund-Johansen M, Enger PØ, Winkler F, Ritter CA, Niclou SP, Watts C, Bjerkvig R, Miletic H. EGFRvIII mutations can emerge as late and heterogenous events in glioblastoma development and promote angiogenesis through Src activation. Neuro Oncol. 2016;18(12):1644–55.
27. Tilak M, Holborn J, New LA, Lalonde J, Jones N. Receptor tyrosine kinase signaling and targeting in glioblastoma multiforme. Int J Mol Sci. 2021;22(4):1831.
28. Iwadate Y. Epithelial-mesenchymal transition in glioblastoma progression. Oncol Lett. 2016;11(3):1615–20.
29. Mecca C, Giambanco I, Donato R, Arcuri C. Targeting mTOR in glioblastoma: rationale and preclinical/clinical evidence. Dis Markers. 2018;2018:9230479.
30. Finch A, Solomou G, Wykes V, Pohl U, Bardella C, Watts C. Advances in research of adult gliomas. Int J Mol Sci. 2021;22(2):924.
31. Maklad A, Sharma A, Azimi I. Calcium signaling in brain cancers: roles and therapeutic targeting. Cancers. 2019;11(2):145.
32. Bosma I, Reijneveld JC, Douw L, Vos MJ, Postma TJ, Aaronson NK, Muller M, Vandertop WP, Slotman BJ, Taphoorn MJB, Heimans JJ, Klein M. Health-related quality of life of long-term high-grade glioma survivors. Neuro Oncol. 2009;11(1):51–8.
33. Petridis AK, Wedderkopp H, Hugo HH, Maximilian Mehdorn H. Polysialic acid overexpression in malignant astrocytomas. Acta Neurochir (Wien). 2009;151(6):601–3 (discussion 603-4).
34. Jin Y, Kim SC, Kim HJ, Ju W, Kim YH, Kim H-J. Increased sialylation and reduced fucosylation of exfoliated cervical cells are potential markers of carcinogenesis in the cervix. Clin Chem Lab Med. 2016;54(11):1811–9.
35. Ferreira IG, Pucci M, Venturi G, Malagolini N, Chiricolo M, Dall'Olio F. Glycosylation as a main regulator of growth and death factor receptors signaling. Int J Mol Sci. 2018;19(2):580.
36. Matsumoto K, Yokote H, Arao T, Maegawa M, Tanaka K, Fujita Y, Shimizu C, Hanafusa T, Fujiwara Y, Nishio K. N-Glycan fucosylation of epidermal growth factor receptor modulates receptor activity and sensitivity to epidermal growth factor receptor tyrosine kinase inhibitor. Cancer Sci. 2008;99(8):1611–7.
37. Zhao Y, Itoh S, Wang X, Isaji T, Miyoshi E, Kariya Y, Miyazaki K, Kawasaki N, Taniguchi N, Gu J. Deletion of core fucosylation on alpha3beta1 integrin down-regulates its functions. J Biol Chem. 2006;281(50):38343–50.
38. Liu CH, Hu RH, Huang MJ, Lai IR, Chen CH, Lai HS, Wu YM, Huang MC. C1GALT1 promotes invasive phenotypes of hepatocellular carcinoma

cells by modulating integrin β1 glycosylation and activity. PLoS One. 2014;9(8): e94995.
39. Ma J, Chen T, Wu S, Yang C, Bai M, Shu K, Li K, Zhang G, Jin Z, He F. iProX: an integrated proteome resource. Nucleic Acids Res. 2019;47(D1):D1211–7.

Publisher's Note